Amer. Malac. Bull. **27**: 157-165 (2009)

X-ray quantitative texture analysis on *Helix aspersa aspera* (Pulmonata) shells selected or not for increased weight

Daniel Chateigner[1], Reinier Kaptein[1], and Mathilde Dupont-Nivet[2]

[1]Laboratoire CRISMAT-ENSICAEN, UMR CNRS n°6508, and IUT-Caen, Université de Caen - Basse Normandie, 6 Boulevard Maréchal Juin 14050 Caen, France

[2]INRA, UR544 Unité de Génétique des Poissons, F-78350 Jouy-en-Josas, France

Corresponding author: daniel.chateigner@ensicaen.fr

Abstract: X-ray Quantitative Texture Analysis (QTA) results are examined for the outer aragonitic shell layers of *Helix aspersa aspersa* (Müller, 1774) to probe the relevance of the approach to non-flat surfaces. Two sets of *H. aspersa aspersa* were studied, for a total of 29 samples. Quantitative texture analysis showed that although the nature of the texture present was roughly constant, the textural strength varied significantly among specimens because of biologically inherited surface irregularities. A statistical analysis showed that textural strength exhibited larger standard deviations for snails selected for greater shell weight than for control snails. The *H. aspersa aspersa* aragonite texture is the same as observed in previous studies, with <110> shell growth directions. This texture causes elastic behavior of the mineral part of the shell, which accommodates moderate shear and compression. We furthermore determine that the colored bands at the shell surface were aligned with the <020> crystal directions.

Key words: *Helix* texture, aragonite, shell growth

Quantitative Texture Analysis (QTA) is frequently used to characterize the macroscopic organization of layered crystals in mollusc shells. A high degree of order (or textural strength) has been reported (Hedegaard and Wenk 1998, Chateigner *et al.* 1999), which varies among taxa, with qualitatively identical textures in closely related species (Chateigner *et al.* 2000). In a single specimen, textures can vary with location in the shell, either between different layers as in *Cypraea testudinaria* (Linnaeus, 1758) (Chateigner *et al.* 1996) or in the same layer, *e.g.*, in Pterioida (Zolotoyabko and Quintana 2002, Checa and Rodriguez-Navarro 2005). The organic matrices control the inorganic crystal orientation (Falini *et al.* 1996) and the crystal shapes themselves (Aizenberg *et al.* 1996), but these two traits can be seen as non-redundant characters in terms of phylogeny. For instance, it has been demonstrated that scanning electronic microscopy images can be misleadingly interpreted in terms of orientation (Chateigner *et al.* 2000). QTA has also been proposed to link living species to extinct fossils in the Bivalvia (Chateigner *et al.* 2002).

Two types of QTA have been applied to the Mollusca in the literature, which differ in the radiation used, thereby probing different material scales. While X-ray diffraction was formerly used (Chateigner *et al.* 1996, 1999, 2000, 2002, Hedegaard and Wenk 1998), Electron Backscatter Diffraction (EBSD) has more recently provided a way for local characterization of texture variation in molluscs (Checa *et al.* 2005, Rousseau *et al.* 2005). Dealing with X-ray analysis using whole X-ray diffraction profiles accounts for all the crystallites, even the smallest ones. However, the X-ray beam extends on the specimens' surface for several mm^2 during the measurements. This simple fact alters the results because of the irregular surface of specimens and prevents quantitative results. Only once in the literature have QTA measurements been made on two specimens of the same species, *Helix aspersa*, and these indicated variability in the quantification of the texture although qualitatively, orientations were the same (Chateigner *et al.* 2000).

Quantitative variation in the results (*e.g.*, variation in textural strength) could also come from real variation in specimen textures, for instance due to a growth anomaly, rather than from an artifact from the irregular irradiation of the surface. These two latter effects could also be explained by the natural texture variation inherent to a species reared in different conditions. In Europe, snail production has increased considerably in the last two decades. Snail farming could give rise to modifications of shell growth that could be undesirable from an economical point of view. In particular, rearing larger snails for an increased tissue weight could modify the shell texture because of the faster growth (Dupont-Nivet *et al.* 2000b). In turn, the texture modifications could affect other shell characteristics (mechanical properties, colors, etc.).

Here we statistically analyzed X-ray QTA results of outer aragonitic layers of *Helix aspersa aspersa* shells, obtained under controlled conditions to optimize growth. Our first aim was to examine a potential effect of the selection method used to increase weight on the degree of preferred orientation.

We then determined the distribution of QTA results on equally shaped samples to show how this distribution changed in two lines of animals, one selected for growth and the other not. Both lines were reared in the same environmental conditions. Our second aim was to exemplify how QTA results can vary between individuals when using X-ray investigations of texture, using the usual measurement characteristics. The certification of the methodology allowed further identification of alignment of given crystal axes with specific shell directions, such as in between shell layers and with colored bands.

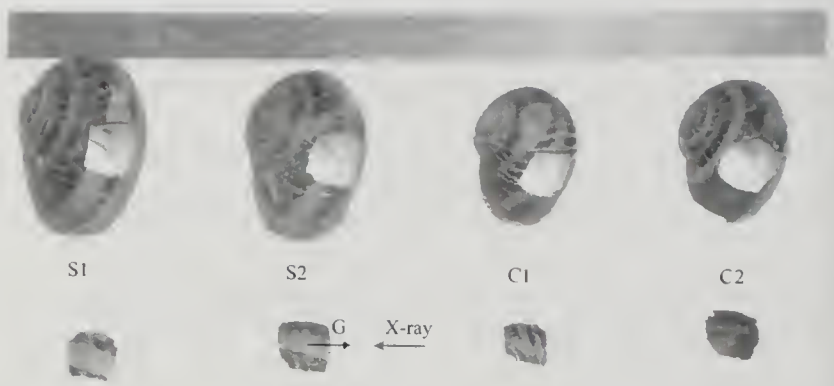

Figure 1. Shell samples used for X-ray measurements. S-specimens come from a line selected for increased weight while C-specimens were control samples. The arrows indicate the growth direction **G** that guides sample positioning with respect to the X-ray beam.

MATERIALS AND METHODS

The specimens of *Helix aspersa aspersa* used in these experiments were from two lines: one selected for increased weight (S) and a control line (C). In the S line, at each generation, the largest snails were chosen for reproduction while in the C line, breeders were chosen at random. The selection procedure is further described in Dupont-Nivet *et al.* (2000b). Animals were all reared in the same room with environmental conditions optimal for growth (density, food, temperature, relative humidity, and photoperiod) as detailed elsewhere (Dupont-Nivet *et al.* 1998, 2000a). Selected snails used in this experiment were from the 7th generation. Their mean weight was 16.98 g versus 10.61 g for the control snails. We collected 'adult' snails, *i.e.*, snails for which the peristome was reflected and, thus, shell growth was completed. Fourteen and fifteen samples were analyzed for the C and S lines, respectively. They were chosen from the whole population available, with weight and age close to the population means, *i.e.*, at a similar growth stage. Shell specimens were all prepared the same day according to the following procedure. Animals were frozen at –18 °C, thawed after one day, and the body manually separated from the shell. Shells were washed with water and air-dried.

For the X-ray QTA experiments, a sample of approx. 1 × 1 cm^2 was cut out the mollusc shells about 0.5 cm from an omnipresent growth irregularity near the macroscopic margin of the shell (Fig. 1). The position of the sample on the diffractometer was as in Chateigner *et al.* (1999). The pole figure plotting was with the projection normal as the **N** direction of the shell, with the **G** and **M** directions respectively vertical and horizontal in the pole figure projection planes (Fig. 2).

The *Helix aspersa aspersa* shell is composed typically of 95% crystallized biogenic aragonite, and of approx. 5% in volume of residual materials, mainly intercrystalline and intracrystalline biomolecules. However, these two latter components are not visible and do not perturb the X-ray diffraction diagrams because of their weak presence and scattering factors and their poor crystallization. Aragonite is one of the three $CaCO_3$ polymorphs and crystallizes in the orthorhombic Pmcn space group with the following cell parameters: a = 4.9611 Å, b = 7.9672 Å, and c = 5.7407 Å for the reference non-biogenic mineral (Pilarti *et al.* 1998).

The X-ray QTA measurements were carried out using a 4-circle diffractometer and a monochromatized Cu-Kα averaged radiation (1.5418 Å) in point focused tube mode (Ricote and Chateigner 2004), with a beam cross-section of 1 × 1 mm^2. The sample was mounted in the center of an Eulerian Cradle (Huber) and rotated in all necessary space directions (at a fixed X-ray incident angle $\omega = 16.64°$, scanning for $0 < \chi < 60°$ and $0 < \phi < 355°$ with 5° steps). Each diagram was acquired for 60 seconds, using the Curved Position Sensitive detector (CPS 120, INEL) which spans all the Bragg diffracted intensities in a 120° 2θ-range at once for all given sample orientations (Fig. 3).

After acquisition, data treatment and QTA involved the so-called "combined analysis" (Chateigner 2004) which used as a first step Rietveld's (1969) refinement of all the 936 resulting diagrams. After this step, integral intensities were

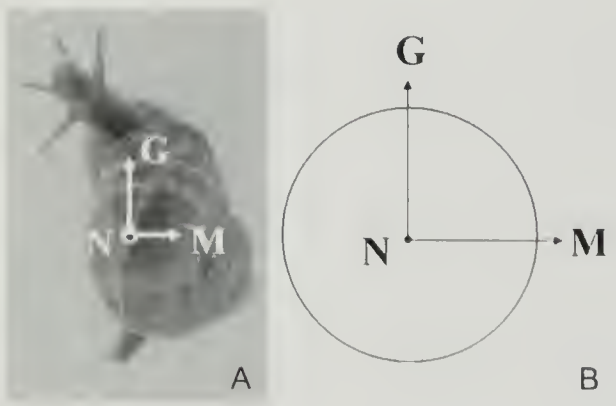

Figure 2. A, Sample reference frame with margin (**M**), growth (**G**), and normal (**N**) directions; B, corresponding pole figure frame.

extracted by the Le Bail extraction procedure (Le Bail *et al.* 1988) and used for quantitative texture analysis with the E-WIMV algorithm (Lutterotti *et al.* 2004). During this latter step, the Orientation Distribution Function (ODF) (Matthies *et al.* 1987) was refined. These steps were iterated 4 times to find the best solution at the convergence of the program, after which pole figures were reconstructed. Instrumental aberrations were calibrated on a standard LaB_6 powder from NIST (SRM660b) and de-convoluted for all the acquired data. Defocusing aberrations with the tilt angle were refined on each sample since they depend on the sample curvature, using a polynomial approach (Chateigner 2004). Pole figures were normalized into orientation density values, expressed in "multiples of random distribution" units (or m.r.d.). In these units, samples without any texture (powders) exhibit homogeneous pole figures at the 1 m.r.d. level, while textured samples show maxima and minima in the pole figures, respectively above and below 1 m.r.d., the former corresponding to the texture components. The E-WIMV approach provided the maximum and minimum values of the ODF, which were quantitative appreciations of the texture strength for specific points of the orientation space. An overall texture strength value was the texture index F^2 (Bunge 1982). During the Rietveld and E-WIMV cycles, the phase cell parameters were also refined, together with other effects that could be detected (crystallite sizes, d-spacing microstrains, stresses, etc). Quality of the results were assessed by the reliability factors for the Rietveld (R_B, R_w, R_{exp}) and ODF (R_{wT}, R_{BT}) refinements, respectively, as defined for this combined analysis (Chateigner 2004) and implemented in the MAUD package (Lutterotti *et al.* 1999).

Scanning Electron Microscope images were obtained from secondary electrons using a Philips XL 30 FEG instrument at an operating voltage of 20 kV. Energy Dispersive Spectrometry could reveal only a single composition with respect to the $CaCO_3$ stoichiometry. Four to five locations were measured for each specimen.

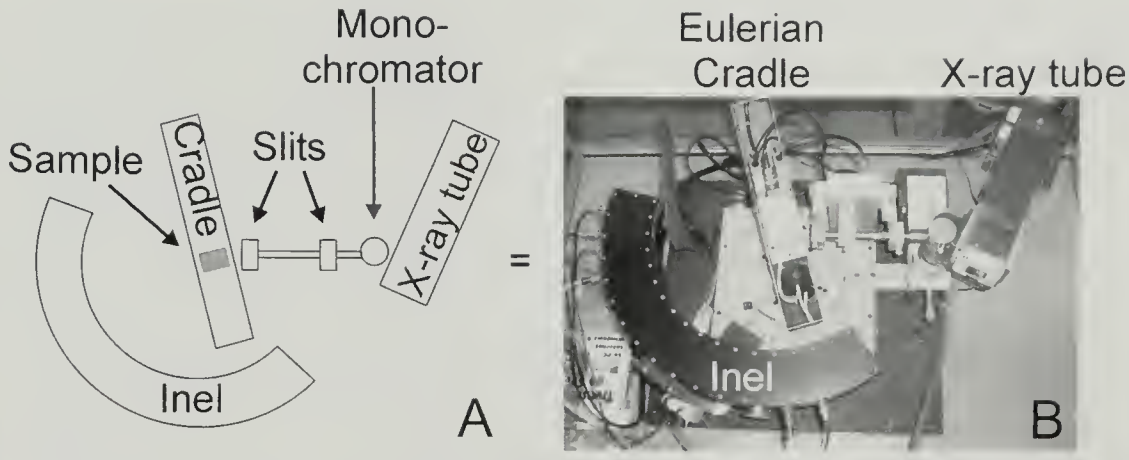

Figure 3. A, Schematic and, B, picture of the X-ray instrumental set-up. Scale: 1: 20.

RESULTS AND DISCUSSION

Individual X-ray diagrams, measured on the same sample for different orientations, clearly showed the unique presence of textured aragonite (Fig. 4). Diagrams measured for different orientations of the sample exhibited different peak intensity ratios, indicating the texture was probably strong. None of these diagrams corresponded to randomly oriented powder. Peak positions corresponded only to the aragonite unit-cell. For this phase and our X-ray energy, the linear absorption coefficient was $\mu = 208\ cm^{-1}$, which corresponded to 99% of the diffracted intensity coming from typically the first 46 μm of the shell, *i.e.*, approx. two thirds of the total shell thickness, then probing the outer, crossed-lamellar layers. For this probe depth the diffraction peaks were very narrow, a signature of well-developed crystallites, to sizes larger than our instrumental limit of typically 1 μm for their mean smallest dimension. No micro-distortion of the d-spacings could be detected, indicating that crystallization occurred in a smooth manner in these layers.

The refinements of both textures (E-WIMV) and structures (Rietveld) were in good agreement with the experimental values as indicated by the reliability factors

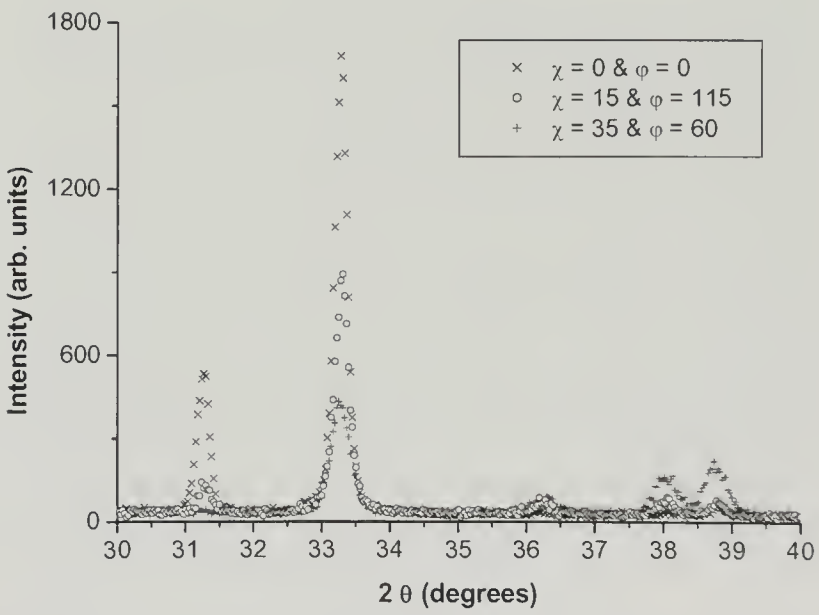

Figure 4. Plot of three spectra measured for three different couples of tilt and azimuth angles, respectively χ and ϕ. The intensity ratio changes as a function of these two rotations, indicating preferred orientation.

(Table 1). On the 29 measured individuals, the Rietveld reliability factors ranged from roughly 14 to 30%, which for 936 diagrams (3×10^6 measured points per sample) was considered as very good, and was also indicated by the low standard deviations ranging between 1 and 2 r.m.s. For the texture refinement (taking out extremes S1-13 and S2-7), reliability factors ranged from approx. 12% to 32% (with 5 to 6 r.m.s. standard deviation) which again were satisfactory for the level of textures shown (Chateigner 2005). Refined cell parameters corresponded to the values of synthetic non-biogenic aragonite, and no difference was observed between the two sample sets within the standard deviations. We conclude selection does not affect aragonite structure. Orientation distribution function minima were all close to 0 m.r.d., indicating that 100% of the total shell volume was textured. Orientation distribution function maxima were very large and fluctuated strongly, with a tendency for larger ODF max in the control samples, even if both sets overlapped within their standard deviations. Variation of the ODF max values reached 35% of the mean value in C samples versus 50% in S. The same maximum variations were visible for the texture index values. Interestingly, standard deviations for texture strengths (ODF max and F^2) were lower for C samples than for S samples. This is particularly significant if we bear in

Table 1. Refinement results from the MAUD package. Grayish specimens represent extreme results (larger texture reliability factors then worst refinements) and have been removed for mean and standard deviation calculations. The standard deviation resulting from the refinements on the parameters is typically 2 units on the last shown digit.

Specimen	R_B (%)	R_w (%)	R_{exp} (%)	R_{BT} (%)	R_{wT} (%)	a (Å)	b (Å)	c (Å)	ODF min (m.r.d.)	ODF max (m.r.d.)	F^2 (m.r.d.)^2
S1-1	21.79	27.70	19.18	18.94	17.33	4.9503	7.9540	5.7410	0.0005	142.00	12.60
S1-3	19.95	25.46	17.39	15.13	13.74	4.9604	7.9760	5.7493	0.0027	160.33	14.45
S1-5	19.88	25.46	17.88	13.39	12.89	4.9680	7.9803	5.7500	0.0006	223.39	20.4
S1-8	20.09	25.97	17.16	15.21	15.35	4.9579	7.9658	5.7438	0.0001	278.05	33.98
S1-9	22.41	28.73	18.45	16.61	15.89	4.9764	7.9956	5.7520	0.0001	252.27	21.97
S1-10	19.52	24.85	19.52	13.79	13.92	4.9672	7.9809	5.7528	0.0344	94.99	7.60
S1-13	17.01	21.44	15.34	13.23	11.74	4.9615	7.9676	5.7408	0.0057	183.23	18.12
S1-14	23.27	30.09	20.90	15.31	13.88	4.9687	7.9813	5.7444	0.0001	191.49	19.62
S1-21	19.83	25.51	17.64	12.77	11.85	4.9579	7.9662	5.7408	0.0002	177.16	24.13
S2-2	20.2	25.77	17.82	13.82	13.26	4.9674	7.9852	5.7453	0.0026	180.38	17.48
S2-3	19.62	25.21	17.60	13.08	12.96	4.9580	7.9740	5.7426	0.0003	206.53	19.58
S2-5	22.72	29.16	17.59	20.62	20.15	4.9559	7.9830	5.7465	0.0154	97.94	9.42
S2-7	20.07	25.12	14.24	36.67	35.8	4.9636	7.9888	5.7409	0.0390	85.40	5.30
S2-11	20.07	28.16	16.79	14.40	14.53	4.9545	7.9627	5.7448	0.0004	142.40	18.61
S211b	22.56	28.85	17.85	19.00	18.35	4.9539	7.9589	5.7433	0.0014	161.01	16.85
Mean	**20.60**	**26.50**	**17.69**	**16.80**	**16.11**	**4.9614**	**7.9747**	**5.7452**	**0.0069**	**171.77**	**17.34**
σ(r.m.s.)	***1.64***	***2.24***	***1.58***	***6.00***	***5.94***	***0.0070***	***0.0118***	***0.0041***	***0.0128***	***47.04***	***7.07***
C1-2	20.73	26.65	17.87	15.08	13.65	4.9561	7.9568	5.7377	0.0081	190.80	15.18
C1-4	19.97	25.53	15.74	22.24	19.32	4.9546	7.9681	5.7420	0.0130	182.90	20.00
C1-6	21.01	26.90	18.17	14.26	13.73	4.9715	7.9833	5.7390	0.0023	173.77	19.32
C1-7	19.59	25.27	17.69	12.63	11.25	4.9553	7.9613	5.7405	0.0016	202.65	28.24
C1-9	22.46	28.72	18.23	16.09	14.73	4.9649	7.9762	5.7395	0.0029	193.19	24.06
C1-11	23.42	29.51	16.46	31.44	28.00	4.9756	7.9829	5.7434	0.0006	166.57	20.27
C1-12	22.83	29.66	18.23	14.84	13.14	4.9664	7.9795	5.7417	0.0008	189.94	25.92
C1-17	19.31	24.8	16.74	15.96	14.52	4.9614	7.9741	5.7397	0.0053	150.38	16.3
C1-23	19.43	24.68	15.82	19.40	22.15	4.9691	7.9867	5.7542	0.0082	266.34	24.23
C2-5	22.23	28.48	17.30	18.67	16.91	4.9579	7.9576	5.7400	0.0003	217.91	27.95
C2-6	20.21	26.05	17.75	13.52	13.68	4.9524	7.9619	5.7382	0.0003	272.31	24.79
C2-7	20.09	25.81	17.67	14.29	12.57	4.9547	7.9518	5.7364	0.0034	163.58	15.07
C2-14	21.57	27.37	16.93	20.25	17.17	4.9560	7.9677	5.7436	0.0009	184.00	22.74
C2-19	20.66	26.48	15.91	18.02	17.88	4.9547	7.9685	5.7406	0.0019	168.25	18.72
Mean	**20.97**	**26.85**	**17.18**	**17.62**	**16.54**	**4.9608**	**7.9697**	**5.7412**	**0.0035**	**194.47**	**21.65**
σ(r.m.s.)	***1.33***	***1.67***	***0.91***	***4.86***	***4.58***	***0.0074***	***0.0110***	***0.0043***	***0.0038***	***36.07***	***4.45***

mind that S samples were flatter than C's, and consequently should have provided less fluctuating X-ray results. Histograms of the F^2 fluctuations are presented for S (Fig. 5A) and C (Fig. 5B) samples, respectively. The error bars on these diagrams are standard deviations. One can clearly notice the reduced variability of F^2 on C samples.

The significantly stronger textures observed for control shells underlined the higher degree of orientation in control samples. Smaller standard deviation of F^2 and ODF max in C compared to S indicated a larger textural resemblance among the control specimens than in the ones selected for increased weight. This could be attributed to the larger shells obtained by selection, which implies a faster, less acute, crystallographic growth.

The overlap of the results (including standard deviations) indicated that the overall preferred crystallite orientation was only mildly dependent on the selection carried out although

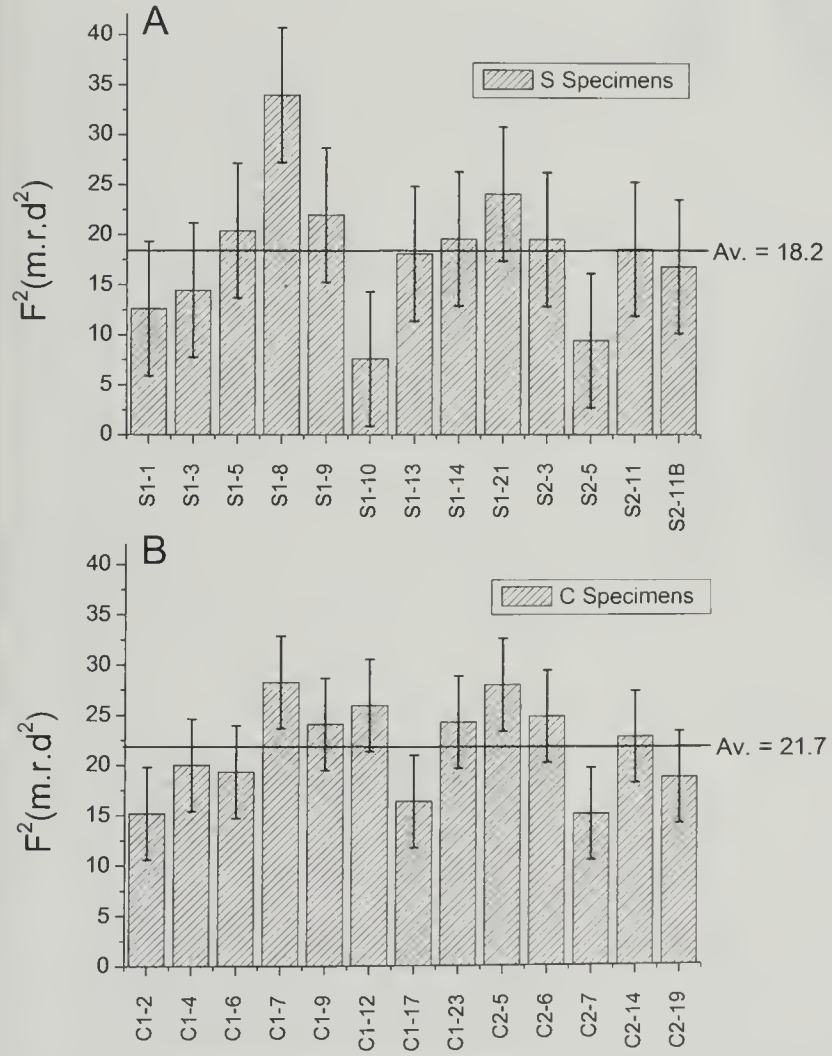

Figure 5. A, F^2 histogram for S (S2-7 omitted) specimens with an average (Av.) of 18.2 m.r.d.^{2}, including an error bar indicating the standard deviation for the entire class: 6.7 r.m.s. and B, F^2 histogram for C (C1-11 omitted) specimens with an average of 21.7 m.r.d.^{2} including an error bar indicating the standard deviation for the entire class: 4.5 r.m.s.

the degree of this orientation was slightly influenced. To better visualize the influence of selection, one can calculate (Fig. 6) the {020} and {002} pole figures for the extremes as well as for an average sample (C2-14, the closest to the F^2 average value) including their minimum and maximum pole distribution values.

This figure shows that the same mean preferred-orientation components were present in the samples, including the extreme samples: QTA provided reliable results although the maximum densities were subjected to deviations due to surface effects like roughness, flatness, and growth anomalies. The textures stabilized corresponded to crystallite **c**-axes (revealed by the {002} pole figures) aligned with the macroscopic normal of the shell, while the **b**-axes (revealed by the {020} pole figures) of aragonite were mainly aligned at approx. 10° from **G**. Slight variations between samples included the error created by positioning the samples on the diffractometer. However, the **b**-axes were always found at this 10° angle from **G**, certifying our positioning. The full width at half maximum of the **c**-axes distribution was around 20° in the direction of the **b**-axes and around 10° perpendicularly.

The fact that all samples exhibited pole figures which had the same shape but different maximum ODF values (and F^2 values) indicated that the direction of the preferred orientation of the crystallites did not change with selection, but the number of crystallites that oriented within a given width of distribution did. Indeed, the non-oriented part of the irradiated samples was in practice zero for all specimens in both C and S sets (Table 1), but the maxima for S were more variable than for control specimens, indicating that selection for larger size induced order-disorder fluctuations of the aragonite layers throughout the population. Adult age, *i.e.*, time to complete growth (until the peristome was reflected), was not significantly different between lines (Dupont-Nivet *et al.* 2000b). This means that larger size in S snails was achieved only through faster growth, with 60% more weight in S animals in the same growing time. The fact that the preferred orientation of crystallites changed only slightly with selection showed that this was a phenomena which was determined more by the species than by growth conditions. However, the faster growth seemed to have potentially unfavorable effects through order-disorder fluctuations of the aragonite layers. Other experiments showed that neither mortality nor shell shape or shell proportion (ratio between shell and animal weight) differed significantly between both lines (Dupont-Nivet, pers. comm.).

Preferred orientations also condition mechanical properties of aggregates, in particular when the constituting crystals possess strong anisotropy of their elastic stiffness constants, as for aragonite. The elastic mechanical behavior of the mineral aragonite fraction can be simulated from the ODF-weighted average of the single crystal stiffness tensor,

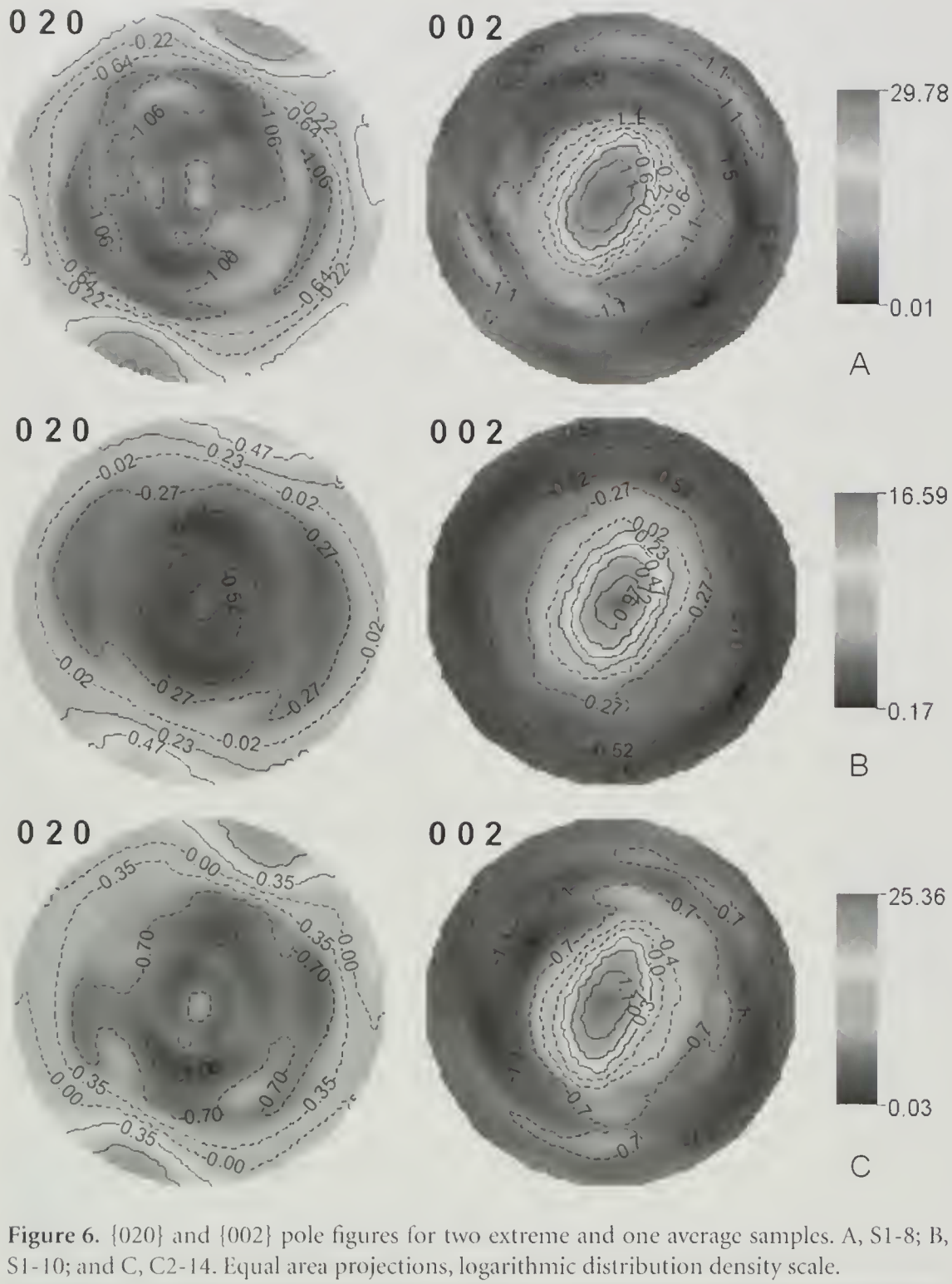

Figure 6. {020} and {002} pole figures for two extreme and one average samples. A, S1-8; B, S1-10; and C, C2-14. Equal area projections, logarithmic distribution density scale.

under the hypothesis of regular grain boundary behaviors, using the geometric mean approach (Ouhenia *et al.* 2008). In such an approach, we ignore the biocomposite nature of the shell and organic-inorganic interactions, and illustrate how the mineral part of the shell affects elastic behavior of the *Helix aspersa aspersa* shell. For an aragonite single crystal there are 9 independent values for the c_{ij} stiffness values (in GPa): c_{11} = 159.58, c_{22} = 86.97, c_{33} = 85.03, c_{44} = 41.32, c_{55} = 25.64, c_{66} = 42.74, c_{12} 36.63, c_{13} = 1.97, and c_{23} = 15.91. In the frame of this calculation, axes 1, 2, and 3 for i and j indices are the **M**, **G**, and **N** directions, respectively. Using the ODF geometric mean, we obtained mean macroscopic stiffness values of (in GPa): c^{M}_{11} = 117, c^{M}_{22} = 107, c^{M}_{33} = 86, c^{M}_{44} = 36, c^{M}_{55} = 34, c^{M}_{66} = 41, c^{M}_{12} = 31, c^{M}_{13} = 14, and c^{M}_{23} = 15, within 6% of the standard deviation, and no significant difference occurred between mean values for the S and C sample sets. Several orientation effects on the macroscopic constants of the shell, compared to the single crystal values, kept the c_{33} constant practically unchanged around 85 GPa. This is because of the strong c-axis orientation with **N**. However, the texture imposes an average value for c^{M}_{11} and c^{M}_{22}, intermediate values compared to the single crystal. This causes a homogeneous mechanical response of the mineral part for compression in the (**G**, **M**) plane of the shell. All the off-diagonal c_{ij} coefficients are homogenized, being much less anisotropic than in the single crystal, giving rise to moderate anisotropic transverse strains in the shell. Because of this, c^{M}_{13} is 7 times larger than in a single crystal, at only a small expense of c^{M}_{12}. The shear coefficients c^{M}_{44}, c^{M}_{55}, and c^{M}_{66} were balanced compared to the single crystal values, and in particular c_{44} and c_{55}. This allows the shell to accommodate relatively large shear coefficients along all directions. Hence, from an elastic anisotropic theory point of view, the strong texture exhibited by the *H. aspersa aspersa* shell behaves, at least for the mineral part, in an optimal manner relative to moderate compressive and shear forces. This is caused by balanced weak and strong elastic coefficients that are not optimal in all macroscopic directions of the shell as observed for instance in the marine gastropod *Charonia lampas lampas* (Linnaeus, 1758) (Ouhenia *et al.* 2008).

One of our objectives was to determine if growth selection had important detrimental effects on shell characteristics. Indeed, even if it is not a selected trait, shell strength is a key point in snail farming. Animals are often manipulated (structure changes, sorting, collecting) which creates multiple chances for shell fracture. These broken shells are problematic for snail survival (dehydration) and growth, and also for the commercial value of animals. The results of this study clearly show that selection did not compromise shell structure, at least in our experimental conditions. However, any side effects

of faster growth should be checked on a regular basis. Moreover, we should check changes in shell thickness and measured shell strength and correlate them with crystallographic results to test if order-disorder fluctuations of the aragonite layers have unfavorable effects.

Looking at a local scale, the crystal organizations on SEM images, the different orientations of crystallites can be made visible. From the shell top ((**G**, **M**) plane) *Helix aspersa aspersa* has successively alternating lamellae (Fig. 7). The crystals are elongated alternatively along a direction at ~ −62° (arrow) from the vertical direction (**G**) and a direction of about 53° from it. This results in a counterclockwise angle between the respective elongations of ~115° in the two succeeding elongation directions.

The two main visible directions of crystal elongation showed a striking angular correspondence between the (110) and (-110) crystallographic planes within aragonite (or between the [110]* and [-110]* reciprocal crystallographic directions, respectively normal to the (110) and (-110) planes). Calculating the angles between (100) and (-110) planes using the cell-parameters (a = 4.96 Å and b = 7.97 Å), one finds an angle of ~116°. When looking at the {110} pole figure (Fig. 8A), the two directions of crystal elongation in the two *Helix aspersa aspersa* layers clearly could be identified to the [110]* and [-110]* crystalline directions (Fig. 8B). However, this does not mean that crystallographic alignment occurred with two components of orientation. Indeed, looking at Fig. 6C, only one, previously described orientation component was present throughout the shell, which corresponded to the {110} four-fold multiplicity of Fig. 8A.

We conclude that elongation of the crystals is operated along the {110} plane of stacking directions. From one layer to the next, this biologically driven growth of crystals occurred without loss of crystallographic orientation, but with change in for individuals selected for growth from one of the {110} planes (for instance (110)) to the other (*e.g.*, (-110)). This is a different growth scheme than observed in the gastropod *Cypraea testudinaria* (Linnaeus, 1758), in which the crossed lamellae of either the radial or co-marginal layers were obtained by a twinning relationship (Chateigner *et al.* 1996). In *Helix aspersa aspersa*, we always found the same single-components of orientation whatever the size of the shell, *i.e.*, whatever the thickness probed, indicating all the layers do keep the crystal orientation. This appears a common pattern in land snails, the same textures having been observed in *Helix pomatia* (Linnaeus, 1758), *Helmintoglypta* (Binney, 1897), and *Englandina* (Férussac, 1818) (Chateigner *et al.* 2000) while all the marine gastropods analyzed to date showed orientation modifications from layer to layer (Chateigner *et al.* 1996, 2000, Checa and Rodriguez-Navarro 2005).

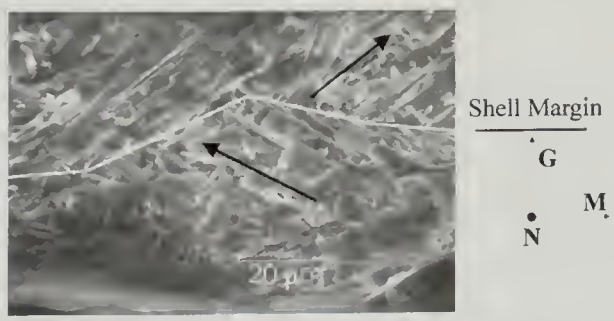

Figure 7. SEM photograph of a fractured *Helix aspersa aspersa* shell parallel to the (**G**, **M**) plane. Magnification is 742 ×. The bottom of the image corresponds to the outermost CCL (Comarginal Crossed-Lamellar) layer while the top of the image is the next inner RCL (Radial Crossed-Lamellar) layer. Arrows illustrate the main crystal directions in the two layers. The shell frame is indicated on the right.

Finally, looking at brownish bands on the surface of *Helix aspersa aspersa* shells (Figs. 1-2), these typically made an angle around 10° with the growth direction **G**. Such angular values were retrieved between the <020> crystallographic directions and **G** ({020} pole figure (Fig. 6C and Fig. 8B)). A close directional relationship may exist between the alignment of the colored bands at the shell surface and the <020> crystallographic directions, using for instance pending bonds from the carbonate groups as they coincide with the observed orientations (Fig. 8C). Such bands were recently associated in *Helix aspersa aspersa* to the presence of un-substituted, methyl terminated chains of 8-13 conjugated double-bond polyenes, either isolated or bound to other molecules, the density of which rendered the color intensity (Hedegaard *et al.* 2006). Since crystallographic texture in molluscs is associated with inter-crystalline macromolecule interaction, the fact that the colored bands of *H. aspersa aspersa* were linked to the specific [020] direction indicates bound polyenes or pigments in this species.

In conclusion, comparison of QTA results of 29 specimens of *Helix aspersa aspersa*, using a statistical analysis, indicated quantitative agreement within standard deviations of ~5 m.r.d.^{2} for the texture index and 40-50 m.r.d. for the maximum value of the orientation distribution function, suggesting such standard deviations vary from about 20 to 35%. We observed a difference between control specimens and the ones selected for larger size: growth stimulation affects the preferred orientations. The standard samples have a higher average texture index with less variability (lower standard deviation). These results indicated the degree to which one can see texture variation between individuals, at least for *H. aspersa aspersa* having a quite regular but curved shell shape.

A clear identification of the elongation direction of the individual crystals in the radial and co-marginal crossed lamellar layers indicated <110> crystallographic directions whatever the layer, while the crystals in different layers all had the same orientation. The colored bands at the surface of the shells were linked to the **b**-axis of the aragonite structure. The elastic behavior of the mineral part of the shell is averaged by

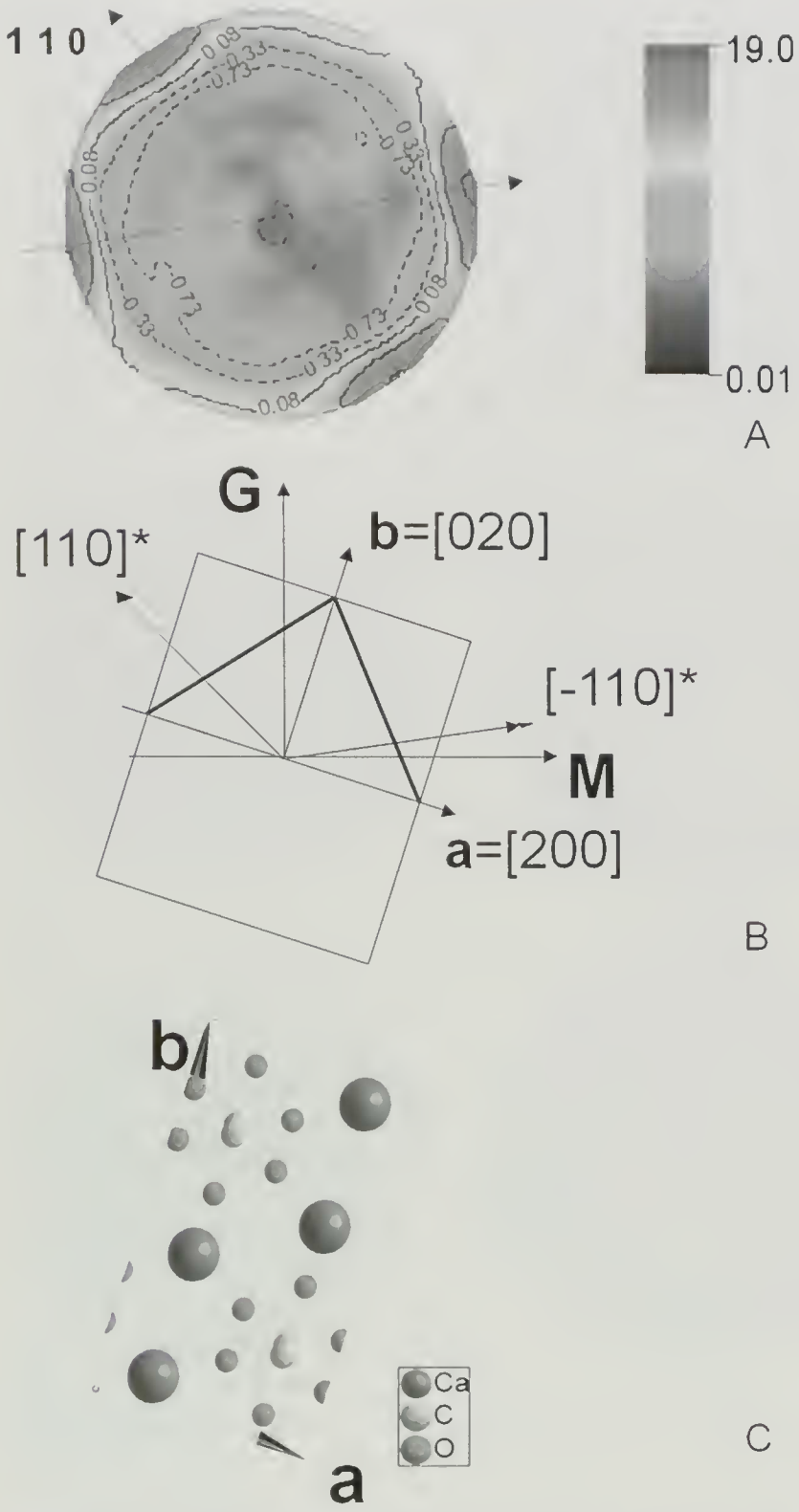

Figure 8. A, {110} pole figure of *Hexlix aspersa aspersa* C2-14; B, schematic of the corresponding main crystalline directions; and C, one theoretical aragonite unit-cell in the (**G**, **N**, **M**) shell reference frame.

the crystallite dispersions to accommodate moderate shear and compression stresses.

ACKNOWLEDGMENTS

The authors would like to thank the French Région Basse-Normandie for its partial funding of the X-ray texture instrument and Hélène Rousselière for the SEM analysis. The two anonymous referees are greatly acknowledged for their constructive comments which contributed to greatly improve the outline of the paper.

LITERATURE CITED

Aizenberg, J., M. Ilan, S. Weiner, and L. Addadi. 1996. Intracrystalline macromolecules are involved in the morphogenesis of calcitic sponge spicules. *Connective Tissue Research* **34:** 255-261.

Bunge, H. J. 1982. *Texture Analysis in Materials Science: Mathematical Methods* (translated by P. R. Morris). Butterworths, London.

Chateigner, D. 2004. Combined analysis: Structure-texture-microstructure-phase-stresses-reflectivity determination by x-ray and neutron scattering. Available at: http://www.ecole.ensicaen.fr/~chateign/texture/combined.pdf 28 April 2009.

Chateigner, D. 2005. Reliability criteria in Quantitative Texture Analysis with experimental and simulated orientation distributions. *Journal of Applied Crystallography* **38:** 603-611.

Chateigner, D., C. Hedegaard, and H. R. Wenk. 1996. Texture analysis of a gastropod shell: *Cypraea testudinaria*. *In*: Z. Liang, L. Zuo, and Y. Chu, eds., *Textures of Materials ICOTOM-11: Proceedings of the 11th International Conference on Textures of Materials, Xi'an, China, 1996.* Academic Publishers. Pp. 1221-1226.

Chateigner, D., C. Hedegaard, and H. R. Wenk. 1999. Quantitative characterisation of mollusc shell textures. *In*: J. A. Szpunar, ed., *Textures of Materials,* Vol. 2. NRC Research Press, Ottawa. Pp. 1495-1500.

Chateigner, D., C. Hedegaard, and H. R. Wenk. 2000. Mollusc shell microstructures and crystallographic textures. *Journal of Structural Geology* **22:** 1723-1735.

Chateigner, D., M. Morales, and E. M. Harper. 2002. QTA of prismatic calcite layers of some bivalves, a link to trichite ancestrals. *Materials Science Forum* **408-412:** 1687-1692.

Checa, A. and A. Rodriguez-Navarro. 2005. Self-organisation of nacre in the shells of *Pterioida* (Bivalvia: Mollusca). *Biomaterials* **26:** 1071-1079.

Dupont-Nivet, M., J. Mallard, J. C. Bonnet, and J. M. Blanc. 1998. Quantitative genetics of reproductive traits in the edible snail *Helix aspersa* Müller. *Journal of Experimental Zoology* **281**: 220-227.

Dupont-Nivet, M., J. Mallard, J. C. Bonnet, and M. J. Blanc. 2000a. Direct and correlated responses to individual selection for large adult weight in the edible snail *Helix aspersa* Müller. *The Journal of Experimental Zoology* **287:** 80-85.

Dupont-Nivet, M., V. Coste, P. Coinon, J. C. Bonnet, and M. J. Blanc. 2000b. Rearing density effect on the production performance of the edible snail *Helix aspersa* Müller in indoor rearing. *Annales Zootechniques* **49:** 447-456.

Falini, G., S. Albeck, S. Weiner, and L. Addadi. 1996. Control of aragonite or calcite polymorphism by mollusk shell macromolecules. *Science* **271:** 67-69.

Hedegaard, C. and H. R. Wenk. 1998. Microstructure and texture pattern of mollusc shells. *Journal of Molluscan Studies* **64:** 133-136.

Hedegaard, C., J. F. Bardeau, and D. Chateigner. 2006. Molluscan shell pigments: An *in-situ* resonance Raman study. *Journal of Molluscan Studies* **72:** 157-162.

Le Bail, A., H. Duroy, and J. L. Fourquet. 1988. *Ab-initio* structure determination of $LiSbWO_6$ by X-ray powder diffraction. *Material Research Bulletin* **23:** 447-452.

Lutterotti, L., S. Matthies, and H. R. Wenk. 1999. National Research Council of Canada, Ottawa. Available at: http://www.ing.unitn.it/maud/ 28 April 2009.

Lutterotti, L., D. Chateigner, S. Ferrari, and J. Ricote. 2004. Texture, residual stress and structural analysis of thin films using a combined X-ray analysis. *Thin Solid Films* **450:** 34-41.

Matthies, S., G. W. Vinel, and K. Helming. 1987. *Standard Distributions in Texture Analysis*, Vol. 1. Akademie-Verlag, Berlin.

Ouhenia, S., D. Chateigner, M. Belkhir, and E. Guilmeau. 2008. Microstructure and crystallographic texture of *Charonia lampas lampas* shell. *Journal of Structural Biology* **163:** 175-184.

Pilarti, T., F. DeMartin, and C. M. Gramaccioli. 1998. Lattice-dynamical estimation of atomic displacement parameters in carbonates: Calcite and aragonite Ca CO_3, dolomite Ca Mg $(CO_3)^2$, and magnesite Mg CO_3. *Acta Crystallographica* (B) **54:** 515-523.

Ricote, J. and D. Chateigner. 2004. Quantitative microstructural and texture characterisation by X-ray diffraction of polycrystalline ferroelectric thin films. *Journal of Applied Crystallography* **37:** 91-95.

Rietveld, H. M. 1969. A profile refinement method for nuclear and magnetic structures. *Journal of Applied Crystallography* **2:** 65-71.

Rousseau, M., E. Lopez, P. Stempfle, M. Brendle, L. Franke, A. Guette, R. Naslain, and X. Bourrat. 2005. Multiscale structure of sheet nacre. *Biomaterials* **26**: 6254-6262.

Zolotoyabko, E. and J. P. Quintana. 2002. Non-destructive microstructural analysis with depth resolution: Application to seashells. *Journal of Applied Crystallography* **35**: 594-599.

Submitted: 8 April 2008; **accepted:** 26 March 2009; **final revisions received:** 29 April 2009